Karlsruhe Institute of Technology (KIT)

Department of Physics

Institute for Theoretical Physics

Bachelor Thesis

SEARCH FOR COLOR OCTET ELECTRONS AT THE LARGE HADRON COLLIDER

submitted by

Michael Kech

on 14.09.2011

Supervisor

Prof. Dr. D. Zeppenfeld

Advisor

Dr. A. Siodmok

Affidavit

I hereby declare that this bachelor's thesis has been written only by the undersigned and without any assistance from third parties. Furthermore I confirm that no sources have been used in the preparation of this thesis other than those indicated in the thesis itself.

Michael Kech, Karlsruhe, 14.09.2011

Abstract

The manifestation of colored leptons, i.e. color octet electrons (e_8), at the Large Hadron Collider (LHC) is investigated in this thesis. Namely the production of an electron and a positron via t- and u-channel color octet electron exchange ($gg \to e_8 \to e^+e^-$) and the resonant production of a color octet electron ($q\bar{q} \to g \to e\,e_8$) that afterwards decays into an electron (positron) and a gluon are analyzed. In the analysis of the t- and u-channel octet electron exchange it is shown that if the octet electron mass (M_{e8}) is equal to 1 TeV the maximal compositeness scale (Λ) for a 5σ discovery of octet electrons at the LHC (assuming an integrated luminosity of $300\,fb^{-1}$) is approximately 8.5 TeV. For an octet electron mass of 4 TeV a 5σ discovery is possible for compositeness scales up to approximately 4 TeV. In the case of resonant production a 5σ discovery of octet electrons assuming the same integrated luminosity at the LHC is possible for compositeness scales of approximately 120 TeV and 4.35 TeV at octet electron masses of 1 TeV and 4.35 TeV respectively.

Contents

1   INTRODUCTION

The Standard Model (SM) has proven to be a very successful theory of fundamental particles and their interactions but there are still numerous puzzles it cannot resolve. Amongst others there is the quark-lepton symmetry, the fact that their charges form exact multiples, the generation replication, the mass hierarchy and the large number of fundamental particles and free parameters which make the SM unsatisfactory [1]. A theory beyond the SM (BSM) on the one hand has to remedy these and other deficiencies by introducing as few new shortcomings as possible and on the other hand deliver testable assertions (e.g. accurate corrections to SM calculations or the prediction of unseen physics) [1]. Until now, no proposed BSM theory has been conclusively verified. Supersymmetry and the concept of extra dimensions are the most popular BSM approaches but compositeness, which is investigated in this study, is also promising.

Composite models postulate that quarks, leptons and gauge bosons (not necessarily all of them) consist of a set of sub structural particles called preons. This implies that the SM can be considered an effective theory of a composite model in the same way as the nuclear force can be considered an effective theory of the quark model [1, 2, 3]. The immensely strong, presumably confining, preon interaction is assumed to result from a non-abelian gauge theory. Compositeness should explain the generation structure, the similarities in the weak interaction of quarks and leptons and the charge multiplets. The masses of leptons and quarks as well as the Kobayashi-Maskawa matrix should at least in principle result from preon dynamics. Compositeness therefore significantly reduces the amount of free parameters in the SM. As a result of preon interactions many new particles such as leptogluons, leptoquarks, diquarks, dileptons and excited fermions are predicted in the different composite models [4]. To date, there is no evidence for a substructure of the SM particles and none of the predicted new particles have been discovered.

In this study the focus is on the manifestation of color octet electrons, belonging to the leptogluons. To illustrate the origin of color octet leptons a possible fermion-scalar composite model is shortly discussed below.

All preons are assumed to be color triplets. In this scenario a lepton is a bound state consisting of a fermionic preon and a scalar anti-preon and antiquarks consist of a scalar preon and a fermionic preon [1, 2, 5]:

$\nu_e = f_1 \overline{s}_1$, $e = f_2 \overline{s}_1$, $\overline{d} = f_1 s_2$, $\overline{u} = f_2 s_2$

Possible charge assignment and other quantum numbers of the preons are given in Table 1, for more details see [1, 2, 5]. For leptons, the decomposition of the color gives:

$$3 \otimes \bar{3} = 1 \oplus 8$$

For quarks, the decomposition gives:

$$3 \otimes 3 = \bar{3} \oplus 6$$

Therefore, quarks are expected to be accompanied by a color sextet and leptons by a color octet partner. In a three fermion model with color triplet preons the decomposition gives $1 \oplus 8 \oplus 8 \oplus 10$. In this case two color octet and one color decuplet partners are expected.

preon	spin	charge	color
f_1	1/2	1/2	3
s_1	0	1/2	3
f_2	1/2	-1/2	3
s_2	0	-1/6	3

Tab. 1: Spin, electric charge and color of scalar and fermionic preons

Although color octet leptons are predicted in many composite models with colored preons [1] they have not received much attention. In recent papers the resonant color octet electron production at the LHeC [4] and the indirect color octet electron manifestation at next generation linear colliders (CLIC, ILC) [6] were analyzed. In this study the focus is on the manifestation of color octet electrons at the LHC's general purpose detectors (ATLAS, CMS). The production of an electron-positron pair via t- and u- channel color octet electron exchange (Figure 1) and the resonant color octet electron production (Figure 2) are analyzed.

In Section 2 the interaction Lagrangian and corresponding Feynman rules, cross sections as well as the decay width are given. Section 3 attends to the revision of the octet electron model that was implemented into CalcHEP [7] for numerical evaluation. To this end, indirect color octet electron manifestation at the ILC is analyzed and the results are compared to A.N. Akay et al. [6]. Section 4 gives a signal and background analysis of the indirect and the resonant manifestation of color octet electrons at the LHC. In Section 5 the obtained results are discussed.
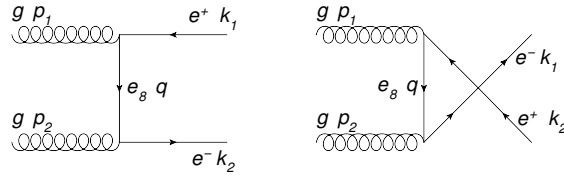
Fig. 1: Feynman diagrams of the processes $gg \to e^+e^-$. p_1, p_2, q, k_1 and k_2 denote four-momenta of corresponding particles. Incoming momenta point into the direction of the corresponding vertex, outgoing momenta point away from it. q points in the direction of the fermion line.
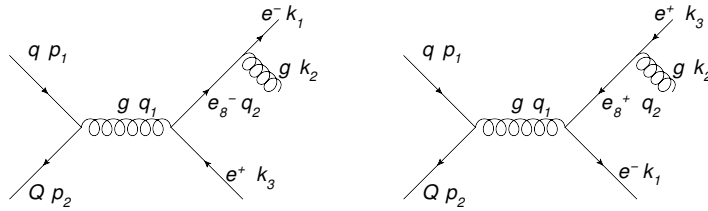
Fig. 2: Feynman diagrams of the processes $gg \to e^+e^-g$. p_1, p_2, q_1, q_2, k_1, k_2 and k_3 denote four-momenta of corresponding particles. All momenta point in the direction of positive time. q represents all quarks except for the top and Q is the corresponding anti-quark.

2 INTERACTION LAGRANGIAN, FEYNMAN RULES, CROSS SECTIONS AND DECAY WIDTH

If quarks and leptons are made of constituents, than at the scale of the constituent binding energies there should appear new interactions among them. At energies below the compositeness scale Λ, these interactions are supressed by inverse powers of Λ. The interaction of color octet leptons (denoted by l_8) with their corresponding lepton (denoted by l) and a gluon is described by the following Lagrangian [6, 4]:

$$L_{Int} = \frac{1}{2\Lambda} \sum_l \bar{\psi}_{l_8} g_s F_{\mu\nu}^a \sigma^{\mu\nu} (\eta_L \psi_{l,L} + \eta_R \psi_{l,R}) + h.c. \tag{1}$$

The sum is performed over all leptons. η_R and η_L are chirality factors, $\psi_{l,R}$ and $\psi_{l,L}$ are right and left handed spinor components of the lepton, $F_{\mu\nu}^a$ is the gluon field strength tensor, $\sigma_{\mu\nu}$ is the antisymmetric tensor and g_s is the strong coupling constant. Chiral invariance of leptons requires $\eta_R \eta_L = 0$. In the following $\eta_R = 0$ and $\eta_L = 2$ is chosen in order to reproduce the results of A. N. Akay et al. [6].

First the couplings for this Lagrangian are derived. The gluon field strength tensor is given by:

$$F_{\mu\nu}^a = \partial_\mu A_\nu^a - \partial_\nu A_\mu^a - g_s f^{abc} A_\mu^b A_\nu^c \tag{2}$$

f^{abc} is the completely antisymmetric tensor of SU(3) and A_μ^a is the gluon field. The Fourier expansion of the fields is given by:

$$A_\mu^a(x) = \int \frac{d^3 k}{(2\pi)^3} \frac{1}{\sqrt{2E_{\bm{k}}}} \sum_\lambda (\epsilon_{\mu,\lambda}(k) a_{a,\lambda}(\bm{k}) e^{-ikx} + \epsilon_{\mu,\lambda}^*(k) a_{a,\lambda}^\dagger(\bm{k}) e^{ikx}) \tag{3}$$

$$\psi_l^a(x) = \int \frac{d^3 p}{(2\pi)^3} \frac{1}{\sqrt{2E_{\bm{p}}}} \sum_s (u_s(p) c_{l,a,s}(\bm{p}) e^{-ikx} + v_s(p) d_{l,a,s}^\dagger(\bm{p}) e^{ikx}) \tag{4}$$

$$\psi_l(x) = \int \frac{d^3 p}{(2\pi)^3} \frac{1}{\sqrt{2E_{\bm{p}}}} \sum_s (u_s(p) c_{l,s}(\bm{p}) e^{-ikx} + v_s(p) d_{l,s}^\dagger(\bm{p}) e^{ikx}) \tag{5}$$

The notation follows the conventions of Peskin and Schröder [8]. In addition the a in Equation (4) denotes the color index that goes from one to eight. The Lagrangian can be written the following way:

$$L_{int} = L + L^\dagger \tag{6}$$

$$L = \frac{ig_s}{2\Lambda} \sum_l \bar{\psi}_{l_8} (\partial_\mu A_\nu^a - \frac{1}{2} g_s f^{abc} A_\mu^b A_\nu^c) \left[\gamma^\mu, \gamma^\nu \right] (1 - \gamma_5) \psi_l \tag{7}$$

$$L^\dagger = \frac{ig_s}{2\Lambda} \sum_l \psi_l^\dagger (\partial_\mu A_\nu^a - \frac{1}{2} g_s f^{abc} A_\mu^b A_\nu^c)(1 - \gamma_5^\dagger) \left[\gamma^{\nu\dagger}, \gamma^{\mu\dagger} \right] \bar{\psi}_{l_8}^\dagger \tag{8}$$

$$= \frac{ig_s}{2\Lambda} \sum_l \bar{\psi}_l \gamma_0 (1 - \gamma_5) \gamma_0 \left[\gamma^\mu, \gamma^\nu \right] \gamma_0 (\partial_\mu A_\nu^a - \frac{1}{2} g_s f^{abc} A_\mu^b A_\nu^c) \gamma_0 \psi_{l_8} \tag{9}$$

$$= \frac{ig_s}{2\Lambda} \sum_l \bar{\psi}_l (\partial_\mu A_\nu^a - \partial_\nu A_\mu^a - g_s f^{abc} A_\mu^b A_\nu^c)[\gamma^\mu, \gamma^\nu](1 + \gamma_5) \psi_{l_8} \tag{10}$$

First the two parts of the Lagrangian that give rise to three particle vertices are considered:

$$L_1 = \frac{ig_s}{2\Lambda} \sum_l \bar{\psi}_{l_8} \partial_\mu A_\nu^a \left[\gamma^\mu, \gamma^\nu \right] (1 - \gamma_5) \psi_l \tag{11}$$

$$L_2 = \frac{ig_s}{2\Lambda} \sum_l \bar{\psi}_l \partial_\mu A_\nu^a \left[\gamma^\mu, \gamma^\nu \right] (1 + \gamma_5) \psi_{l_8} \tag{12}$$

Clearly $L_2(L_1)$ only contributes in the cases that involve incoming $l_8^- (l_8^+)$ or $l^+(l^-)$ or outgoing $l_8^+ (l_8^-)$ or $l^-(l^+)$. L_1 and L_2 give rise to the vertices shown in Figure 3 and the couplings can be inferred from the following calculation:

$$\langle l^- | i \int d^4x : L_1(x) : | l_8^-, g \rangle \tag{13}$$

$$= \langle l^- | \frac{-g_s}{2\Lambda} \int d^4x \sum_l \bar{\psi}_{l_8} \partial_\mu A_\nu^a [\gamma^\mu, \gamma^\nu](1 - \gamma_5) \psi_l | l_8^-, g \rangle \tag{14}$$

$$= \langle 0| \frac{-g_s}{2\Lambda} \int d^4x \, e^{ikx} \bar{u}_{s_1}(k) \delta_{ab}(-iq_\mu)e^{-iqx}\epsilon_{\nu,\lambda}\delta_{ca}[\gamma^\mu, \gamma^\nu](1-\gamma_5)e^{-ipx}u_{s_2}(p)|0\rangle \tag{15}$$

$$= \bar{u}_{s_1}(k)\frac{-ig_s}{2\Lambda}\delta_{bc}(\gamma^\alpha \slashed{q} - \slashed{q}\gamma^\alpha)(1-\gamma_5)\epsilon_{\alpha,\lambda}u_{s_2}(p)\int d^4x \, e^{i(k-q-p)x} \tag{16}$$
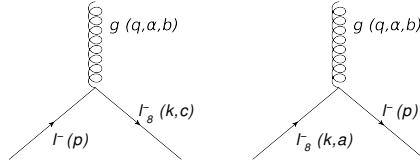
Fig. 3: The left and right vertex correspond to L_1 and L_2 respectively (Eqs. 11 and 12). p, q and k denote four-momenta of appropriate particles. All four-momenta may point in the direction of the vertex. a and b are color indices. s_1 and s_2 denote spin states. κ is the Lorentz index of the gluon field and λ denotes its polarization state.

The coupling derived from L_1 (eq. 11) is given by:

$$i\frac{g_s}{2\Lambda}\delta_{bc}(\slashed{q}\gamma_\alpha - \gamma_\alpha\slashed{q})(1-\gamma_5) \tag{17}$$

An analogous calculation gives coupling derived from L_2 (eq. 12):

$$i\frac{g_s}{2\Lambda}\delta_{bc}(\slashed{q}\gamma_\alpha - \gamma_\alpha\slashed{q})(1+\gamma_5) \tag{18}$$

The derivation of the couplings for the four particle vertices can be found in Appendix B. The octet lepton propagator is given by the fermion propagator multiplied by a Kronecker delta to ensure color conservation:

$$i\frac{\not{p}+m}{p^2-m^2}\delta_{ab} \tag{19}$$

Having obtained the couplings and the propagator, the differential partonic cross sections of the investigated signal processes and the decay width of octet electrons are calculated. First the differential partonic cross section for the indirect manifestation $(gg \to e^+e^-)$ is derived. The matrix elements for the diagrams presented in Figure 1 are given by:

$$M = M_1 + M_2 \tag{20}$$

$$M_1 = \delta_{ab}\bar{u}_{s_2}(k_2)\frac{ig_s}{2\Lambda}(\not{p}_2\not{\epsilon}_2 - \not{\epsilon}_2\not{p}_2)(1+\gamma_5)i\frac{\not{q}+m}{q^2-M_{e_8}^2+i\epsilon}\frac{ig_s}{2\Lambda}(\not{p}_1\not{\epsilon}_1 - \not{\epsilon}_1\not{p}_1)(1-\gamma_5)v_{s_1}(k_1) \tag{21}$$

$$M_2 = \delta_{ab}\bar{u}_{s_1}(k_1)\frac{ig_s}{2\Lambda}(\not{p}_2\not{\epsilon}_2 - \not{\epsilon}_2\not{p}_2)(1+\gamma_5)i\frac{\not{q}+m}{q^2-M_{e_8}^2+i\epsilon}\frac{ig_s}{2\Lambda}(\not{p}_1\not{\epsilon}_1 - \not{\epsilon}_1\not{p}_1)(1-\gamma_5)v_{s_2}(k_2) \tag{22}$$

Neglecting the electron mass and the octet electron decay width, the following expression for the partonic differential cross section is obtained:

$$\frac{d\hat{\sigma}}{d\hat{t}}(gg \to e^+e^-) = \frac{1}{2s}\frac{1}{16\pi\hat{s}}\left\langle|M|^2\right\rangle = \frac{1}{4\pi}\left(\frac{g_s}{\Lambda}\right)^4\left(\frac{\hat{t}^3\hat{u}}{\hat{s}^2(M_{e_8}^2-\hat{t})^2} + \frac{\hat{u}^3\hat{t}}{\hat{s}^2(M_{e_8}^2-\hat{u})^2}\right) \tag{23}$$

$\hat{\sigma}$ is the parton-level cross section, $\hat{s}$, $\hat{u}$ and $\hat{t}$ denote Mandelstam variables and M_{e8} is the mass of the color octet electron. The partonic differential cross section for the inverse process $e^+e^- \to gg$, which is analyzed in Section 2 in order to revise the implementation of the color octet electron model into CalcHEP, is given by:

$$\frac{d\hat{\sigma}}{d\hat{t}}(e^+e^- \to gg) = 32 \cdot \frac{d\hat{\sigma}}{d\hat{t}}(gg \to e^+e^-) = \frac{8}{\pi}\left(\frac{g_s}{\Lambda}\right)^4\left(\frac{\hat{t}^3\hat{u}}{\hat{s}^2(M_{e_8}^2-\hat{t})^2} + \frac{\hat{u}^3\hat{t}}{\hat{s}^2(M_{e_8}^2-\hat{u})^2}\right) \tag{24}$$

In addition to the indirect manifestation also the resonant production of octet electrons is also analyzed. The processes considered are $q\bar{q} \to g \to e_8^{\pm} e^{\mp}$. The octet electron then decays in an electron (positron) and a gluon. The process $gg \to e_8^{\pm} e_8^{\mp}$ is beyond the scope of this thesis and is expected to be insignificant at high octet electron masses since the gluon parton distribution functions are suppressed at high longitudinal momentum fractions of the initial gluons. A similar observation was made by S. Martin [9] in the case of gluino production at the LHC. It is stated that the production of gluinos by gluon-gluon and gluon-quark fusion at the LHC is suppressed at gluino masses higher than 1 TeV. However in order to make more precise statements it is necessary to study the octet electron production by gluon fusion in more detail, which can be done in the future.

Now the cross section for the process $q\bar{q} \to ge^+e^-$ is derived. Figure 2 presents the corresponding Feynman diagrams. The masses of incoming and outgoing particles are neglected.

The matrix element for the first process in Figure 2 is given by:

$$M_1 = \delta_{ab}\bar{v}_{s_2}(p_2) i g_s t^a \gamma^{mu} u_{s_1}(p_1) \frac{i g_{\mu\nu}}{q_1^2} \bar{u}_{r_1}(k_1) \frac{i g_s}{2\Lambda}(-\slashed{k}_2\slashed{\epsilon}_2 + \slashed{\epsilon}_2\slashed{k}_2)$$

$$(1 + \gamma_5)\frac{\slashed{q}_2 + M_{e8}}{q_2^2 - M_{e8}^2 + i\epsilon}\frac{i g_s}{2\Lambda}(\slashed{q}_1\gamma^{\nu} - \gamma^{\nu}\slashed{q}_1)(1 - \gamma_5)v_{r_2}(k_3) \tag{26}$$

Provided that the octet electron width is small the octet electron propagator can be approximated by a delta function. In this limit there is no interference between the two diagrams. The phase space is given by:

$$d\phi_3(p_1, p_2; k_1, k_2, k_3) = \int_0^{\infty} \frac{dM^2}{2\pi}\, d\phi_2(p_1, p_2; q_2, k_3)d\phi_2(q_2; k_1, k_2) \tag{27}$$

$$= \int_0^{\infty} \frac{dM^2}{2\pi} \int d\Omega_3 \frac{1}{16\pi^2}\frac{\hat{s} - M^2}{2\hat{s}} \int d\Omega_1 \frac{1}{32\pi^2} \tag{28}$$

$d\phi_2(p_1, p_2; q_2, k_3)$ is evaluated in the center-of-mass system with the z-axis along the q_2-direction, while $d\phi_2(q_2; k_1, k_2)$ is evaluated in the rest system of q_2 with the z-axis along the q_2-direction. The averaged squared matrix element that corresponds to the first diagram in Figure 2 is given by:

$$\left\langle |M|^2 \right\rangle = \frac{128}{9} \left(\frac{g_s M}{\Lambda} \right)^4 \frac{g_s^2}{\hat{s}^2} \frac{\pi}{M\Gamma} \delta(q_2^2 - M_{e8}^2)(4(p_2 \cdot k_3 p_1 \cdot k_1 + p_1 \cdot k_3 p_2 \cdot k_1)$$

$$-\hat{s}\, k_1 \cdot k_3 + M_{e8}^2 (2k_3 \cdot (p_1 + p_2) - k_3 \cdot k_1) \tag{29}$$

The color factor is $\frac{1}{9} \sum t_{ij}^a t_{ji}^a = \frac{4}{9}$. The averaged squared matrix element of the second process in Figure 2 is obtained by interchanging k_1 and k_3 in Equation (29). The partonic differential cross section for the process $q\bar{q} \to g e^+ e^-$ is given by:

$$\frac{d^2\hat{\sigma}}{d\Omega_1 d\Omega_3}(q\bar{q} \to g e^+ e^-) = \frac{1}{18\pi^3} \left(\frac{g_s^2}{\Lambda} \right)^2 \frac{\hat{s} - M_{e8}^2}{\hat{s}^3}(4(p_2 \cdot k_3 p_1 \cdot k_1 + p_1 \cdot k_3 p_2 \cdot k_1)$$

$$-(\hat{s} + M_{e8}^2)\, k_1 \cdot k_3 + M_{e8}^2(k_3 + k_1) \cdot (p_1 + p_2)) \tag{30}$$

$$= \frac{1}{18\pi} \left(\frac{g_s^2}{\Lambda} \right)^2 \frac{\hat{s} - M_{e8}^2}{\hat{s}^3} [\frac{\hat{s} - M_{e8}^2}{4}(\hat{s}(1 + cos\theta_3)(1 + cos\theta_1) + M_{e8}^2(1 - cos\theta_3)(1 - cos\theta_1)$$

$$-(\hat{s} + M_{e8}^2)(1 + cos\theta_3) + 2M_{e8}^2 + \frac{\sqrt{\hat{s}} M_{e8}}{2} sin\theta_3 cos\phi_3 + \frac{\hat{s} M_{e8}^2}{4}(1 + cos\theta_3) + \frac{M_{e8}^4}{4}(1 - cos\theta_3)] \tag{31}$$

Taking the parton distribution functions into account the total cross section is given by:

$$\sigma_{tot} = \sum_i \int_0^1 dx_{1,i} \int_0^1 dx_{2,i} f_{1,i}(x_{1,i}, q) f_{2,i}(x_{2,i}, q) \hat{\sigma}_i(x_{1,i}, x_{2,i}, q) \tag{32}$$

Finally the decay width is derived. The matrix element for the decay of an octet electron is given by:

$$M = \delta_{ab} \bar{u}_{s_2}(k) \frac{ig_s}{2\Lambda}(-\slashed{q}\slashed{\epsilon} + \slashed{\epsilon}\slashed{q})(1 + \gamma_5) u_{s_1}(p) \tag{33}$$

Neglecting the electron mass, this yields the following decay width:

$$\Gamma_{e8} = \frac{1}{2M_{e8}} \frac{2}{\pi} \frac{M_{e8}^4 g_s^2}{\Lambda^2} = \frac{\alpha_s M_{e8}^3}{\Lambda^2} \tag{34}$$

The calculations presented in this section were used to implement color octet electrons into CalcHEP [7], which is used to numerically evaluate the processes of interest at tree-level, and to afterwards cross-check this implementation. In Appendix A details about the implementation of color octet electrons into CalcHEP are provided.

3 ANALYSIS OF THE T-CHANNEL OCTET ELECTRON SIGNAL AT THE ILC

The main purpose of this section is to confirm that the implementation of color octet electrons into CalcHEP was done correctly by reproducing the results of A. N. Akay et al. [6]. The signal process $e^+e^- \to gg$ is analyzed. The relevant background processes are $e^+e^- \to \gamma, Z \to u\bar{u}, d\bar{d}, s\bar{s}, c\bar{c}, b\bar{b}$. Both t- and u-channel octet electron exchange is considered. All parameters of the ILC relevant for the following calculations are presented in Table 2 [10]. The compositeness scale is put on a level with the color octet electron mass. It is assumed that A. N. Akay et al. also chose $\eta_L = 2$ and $\eta_R = 0$.

$\sqrt{s}$ [TeV]	L [$10^{34}cm^{-2}s^{-1}$]	N [10^{10}]	σ_x [nm]	σ_y [nm]	σ_z [μm]
0.5	2	2	640	5.7	300

Tab. 2: Center-of-mass energy, luminosity and beamstrahlung parameters of the ILC. N is the number of particles in a bunch, σ_x and σ_y are the beam sizes at interaction point and σ_z is the bunch length.

Figures 4, 5 and 6 present normalized invariant mass, pseudorapidity and transverse momentum distributions of both signal and background final state jets. These distributions suggest that the following cuts on final state jets essentially suppress the background without strongly effecting the signal: invariant mass $M > 375$ GeV, pseudorapidity $|\eta| < 1$ and transverse momentum $p_T > 120$ GeV. The obtained distributions are very similar to those of A.N. Akay et al. [6], but the logarithmic scale does not allow an exact comparison. Some further calculations were therefore performed.

M_{e8} [TeV]	0.5	1.0	1.5	2.0
σ_s [pb]	89.83	0.6631	0.003002	0.000318
σ_b [pb]	1.76			

Results of A. N. Akay et al. [6]:

M_{e8} [TeV]	0.5	1.0	1.5	2.0
σ_s [pb]	89.835	0.663	0.0030	0.00032
σ_b [pb]	1.757			

Tab. 3: Signal cross sections (σ_s) at different masses M_{e8} of color octet electron and background cross section (σ_b) for the ILC . The cuts for final state jets are: $M > 375$ GeV, $p_T > 120$ GeV and $|\eta| < 1$. Λ is set equal to M_{e8}.

Table 3 presents the cross sections of background and signal processes at different color octet electron masses for the ILC using the cuts selected above.

To calculate statistical significance the following formula is used [6]:

$$S = \frac{\sigma_s}{\sqrt{\sigma_b + \sigma_s}} \sqrt{L_{int}} \qquad (35)$$

σ_s and σ_b denote the total cut signal and background cross sections and L_{int} is the integrated luminosity. The luminosity integrated over one year is assumed to be $200\,fb^{-1}$ [6]. In Table 4 reachable masses for 2σ exclusion, 3σ observation and 5σ discovery of color octet electrons are presented for one and three years of operation.

years	M_{e8} for 5σ	M_{e8} for 3σ	M_{e8} for 2σ
1	1.64 TeV	1.75 TeV	1.85 TeV
3	1.76 TeV	1.88 TeV	1.98 TeV

Results of A. N. Akay et al.[6]:

years	M_{e8} for 5σ	M_{e8} for 3σ	M_{e8} for 2σ
1	1.640 TeV	1.750 TeV	1.850 TeV
3	1.760 TeV	1.880 TeV	1.980 TeV

Tab. 4: Reachable color octet electron masses for discovery, observation and exclusion at the ILC after one and three years of operation. The cuts on final state jets are: $M > 375$ GeV, $p_T > 375$ GeV and $|\eta| < 1$.

These results conform very well to the ones of A.N. Akay at al. [6] and therefore strongly suggest that color octet electrons were implemented correctly into CalcHEP.
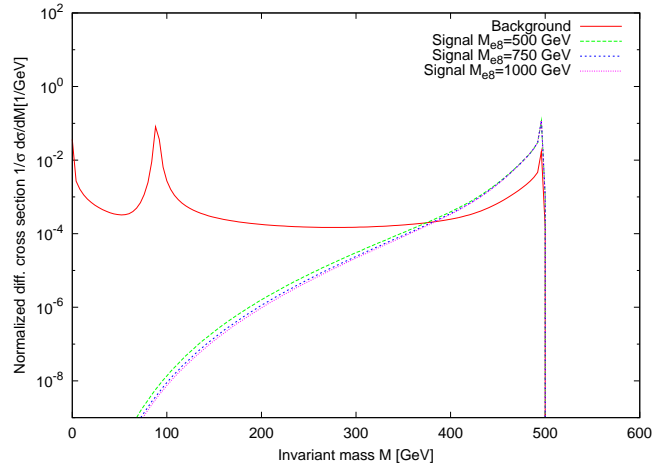
Fig. 4: Normalized invariant mass distribution of final state jets for background and signal.
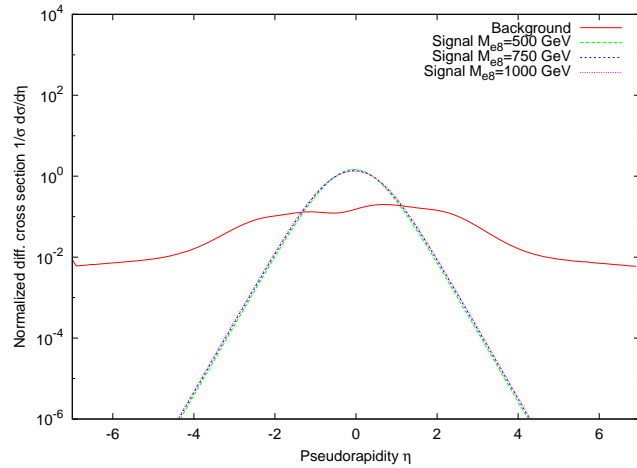
Fig. 5: Normalized pseudorapidity distribution of final state jets for background and signal.
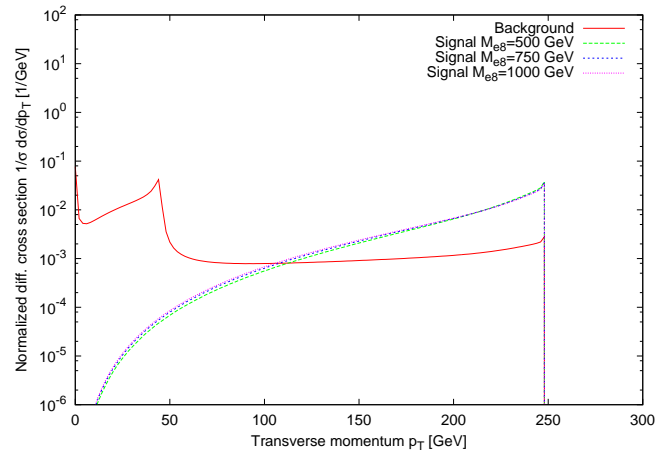
Fig. 6: Normalized transverse momentum distribution of final state jets for background and signal.

4 ANALYSIS OF COLOR OCTET ELECTRON MANIFESTATION AT THE LHC

In contrast to the ILC, CLIC and the LHeC, the LHC is already operating and provides promising oppertunities in the search for BSM particles. Therefore color octet electron manifestation at the LHC's general purpose detectors (ATLAS, CMS) is analyzed. Both the indirect and the resonant manifestation of octet electrons are investigated assuming the center-of-mass energy of the two initial protons to be 14 TeV.

The three major components of the ATLAS detector are the inner tracking detector, the calorimeter and the muon detector. Since in the following electrons, positrons and jets are the only final state objects the muon detector is not of interest. Immersed in a magnetic field of 2 T [11] provided by a superconducting solenoid, silicon pixel and silicon strip detectors covering pseudorapidities of $|\eta| < 2.5$ [11] are used to reconstruct charged particle tracks and vertices. The hermetic calorimeter surrounding the tracker covers pseudorapidities of $|\eta| < 4.9$ [11] and enables the three-dimensional reconstruction of particle showers (jets). The properties of the CMS detector are very similar and the differences do not affect the following calculations. The analysis is targeted to deliver rough estimations and therefore detector simulation is not performed in this study.

4.1 SIGNAL AND BACKGROUND ANALYSIS OF THE T-CHANNEL CONTRIBUTION

In this section the indirect manifestation of color octet electrons at the LHC is analyzed. The signal and background processes considered are $gg \rightarrow e^+e^-$ and $u\bar{u}, d\bar{d}, s\bar{s}, c\bar{c}, b\bar{b} \rightarrow \gamma, Z \rightarrow e^+e^-$ respectively. Both t- and u-channel contributions are considered. The parton distribution function used for the calculations in this thesis is CTEQ6l [12]. In the following the compositeness scale is chosen to be $5000\,\text{GeV}$.

Based on the following motivations some cuts are made in advance. Firstly the invariant mass of the final state electron and positron (both denoted by e) is chosen to be greater than 100 GeV to omit the Z-resonance of the background signal. Secondly the transverse momenta of both the final state electron and the final state positron are required to be greater than 25 GeV, as it is expected that the background signal is dominant at low transverse momenta of final state particles. Since the LHC's

general purpose detectors are only sensitive to leptons with a pseudorapidity between -2.5 and 2.5 both the final state electron and positron pseudorapidities are required to lie within these borders. The distributions presented in the following were created using these cuts. Figure 7 shows the total cross section of the signal as a function of the color octet electron mass. In order to improve the cut selection the transverse momentum as well as the normalized pseudorapidity distributions of the final state lepton and the invariant mass distribution of the final state electron and positron are plotted in Figures 8, 9 and 10 respectively. Using these distributions the following cuts on the final state particles are selected: transverse momentum of the electron $p_T > 500$ GeV ($p_T > 750$ GeV), pseudorapidities of both the electron and the positron $|\eta| < 2.0$ ($|\eta| < 2.0$) and invariant mass of the electron and the positron $M > 1000$ GeV ($M > 1500$ GeV) for masses smaller (higher) than 2800 GeV.

Table 5 presents cross sections of the signal and background for the LHC using the cuts selected above. To analyze the statistical significance, Equation (35) is used. Setting the octet electron mass equal to the compositeness scale the reachable octet electron masses for a 5σ discovery at different integrated luminosities are given in Table 6.
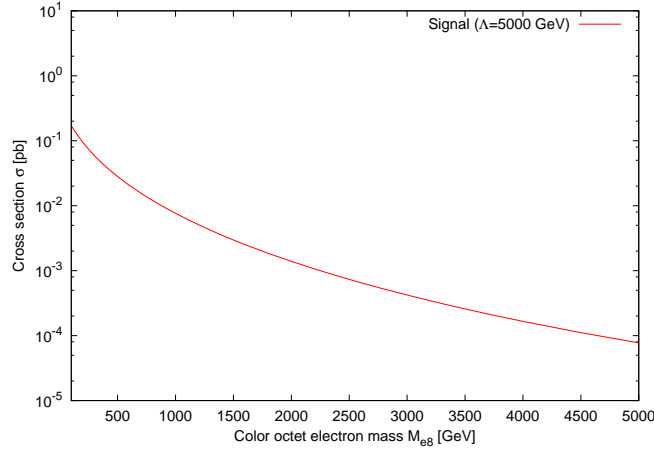
Fig. 7: t- and u-channel octet electron cross section as a function of the octet electron mass. The following cuts on final state leptons are applied: $p_T(e) > 25$ GeV, $|\eta(e)| < 2.5$ and $M(e^-, e^+) > 100$ GeV. The center of mass energy is assumed to be 14 TeV.
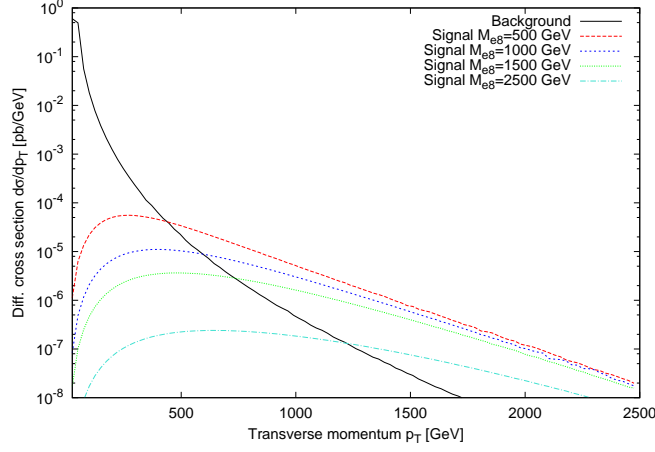
Fig. 8: Transverse momentum distribution of the final state lepton. The compositeness scale is chosen to be 5000 GeV. The center-of-mass energy is assumed to be 14 TeV. The following cuts on final state particles are applied: $p_T(e) > 25$ GeV, $|\eta(e)| < 2.5$ and $M(e^-, e^+) > 100$ GeV.
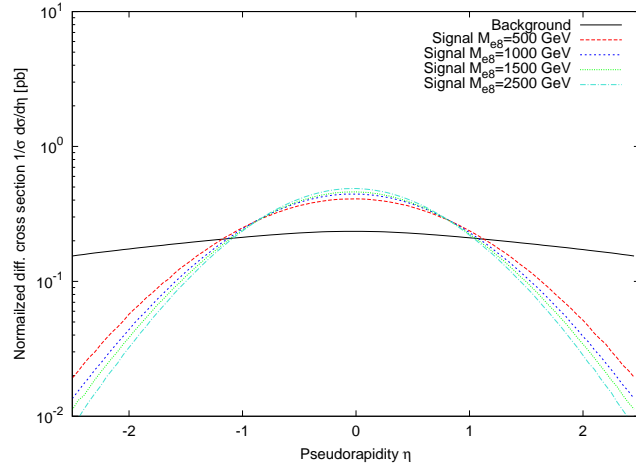
Fig. 9: Normalized pseudorapidity distribution of final state lepton. The compositeness scale is chosen to be 5000 GeV. The center-of-mass energy is assumed to be 14 TeV. The following cuts on final state particles are applied: $p_T(e) > 25$ GeV, $|\eta(e)| < 2.5$ and $M(e^-, e^+) > 100$ GeV.
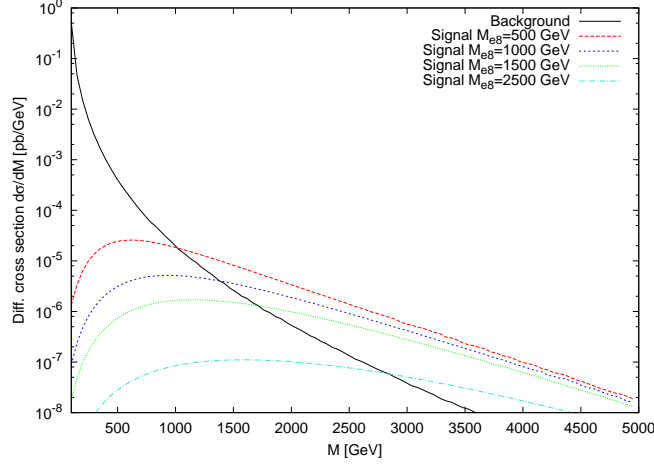
Fig. 10: Invariant mass distribution of the final state electron and positron. The compositeness scale is chosen to be 5000 GeV. The center-of-mass energy is assumed to be 14 TeV. The following cuts on final state particles are applied: $p_T(e) > 25$ GeV, $|\eta(e)| < 2.5$ and $M(e^-, e^+) > 100$ GeV.

M_{e8} [TeV]	0.5	1.0	1.5	2.5
σ_s [fb]	9.42	4.19	1.96	0.555
σ_b [fb]	2.58			

Tab. 5: Signal (σ_s) and background (σ_b) cross sections after cuts for the LHC at different masses M_{e8} of color octet electron. The compositeness scale is chosen to be 5000 GeV. The cuts on final state leptons are: $M_{inv}(e^-, e^+) > 1000$ GeV, $p_T(e) > 500$ GeV and $|\eta(e)| < 2$.

M_{e8} at 10 fb^{-1}	M_{e8} at 30 fb^{-1}	M_{e8} at 100 fb^{-1}	M_{e8} at 300 fb^{-1}
2.80 TeV	3.20 TeV	3.55 TeV	4.00 TeV

Tab. 6: Reachable color octet electron masses for a 5σ discovery at the LHC considering different integrated luminosities. The center of mass energy is assumed to be 14 GeV. The compositeness scale is set equal to the octet electron mass. The cuts on final state leptons are: $M_{inv}(e^-, e^+) > 1500$ GeV, $p_T(e) > 750$ GeV and $|\eta(e)| < 2$.

Figure 11 shows the reachable values of the compositeness scale as a function of the color octet electron mass for a 5σ discovery at different integrated luminosity.
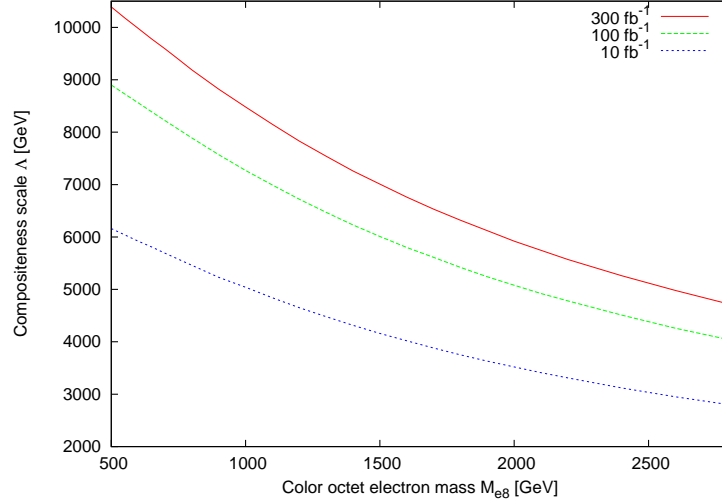
Fig. 11: Reachable compositeness scale over color octet electron mass for a 5σ discovery at different integrated luminosities. The center of mass energy is assumed to be $14\,TeV$. The cuts on final state leptons are: $M_{inv}(e^-, e^+) > 1000$ GeV, $p_T(e) > 500$ GeV and $|\eta(e)| < 2$.

Finally the obtained results at the LHC are compared to the results expected at possible future colliders [4, 6]. Considering the indirect manifestation, the reachable octet electron mass for a 5σ discovery at the LHC is 4.0 TeV assuming an integrated luminosity of $300\,fb^{-1}$ if the compositeness scale is equal to the octet electron mass. This value clearly exceeds the capacity of CLIC1 (1.6 TeV) [6] and the ILC (1.6 TeV) [6] to discover octet electrons and is also well behind CLIC2 (6.4 TeV) [6]. The covered values of the compositeness scale for a 5σ discovery of octet electrons at the LHC is 6.0 TeV for an octet electron mass of 2000 TeV. This compares to $1.3\,TeV$ at both ClIC1 and the ILC [6] and $15\,TeV$ at CLIC2 [6].

4.2   SIGNAL AND BACKGROUND ANALYSIS OF THE RESONANT PRODUCTION

In this section the resonant color octet electron production is analyzed. The maximum reachable compositeness scale for a 5σ discovery at different octet electron masses is estimated. The signal

and background processes considered are presented in Figure 12. Interferences between background and signal processes are neglected, as they are expected to be comparatively small. Requiring the transverse momenta of each the electron, the positron and the jets to be greater than 100 GeV the total signal cross section as a function of the octet electron mass is presented in Figure 13.

Based on the following motivation some cuts are selected to create the distributions presented in Figures 14-16: Firstly the invariant mass of the final state electron and positron is required to be greater than 100 GeV to omit the Z-resonance of the background signal. Secondly the transverse momentum of the final state jets is chosen to be greater than 50 GeV and the transverse momenta of both the final state electron and positron are chosen to be greater than 25 GeV expecting the background to be dominant at low transverse momenta of final state objects. Since the LHC's general purpose detectors are only sensitive to leptons with a pseudorapidity between -2.5 and 2.5 the pseudorapidities of the final state electron and positron are required to lie within these borders. The pseudorapidity of the jets is also chosen to be between -2.5 and 2.5 (the range of the LHC's general purpose detectors includes higher pseudorapidities but most of the signal is expected to be concentrated within these limits). At last the invariant mass of the final state jets and the final state electron is chosen to lie between 475 GeV and 525 GeV (950 GeV and 1050 GeV) for an octet electron mass of 500 GeV (1000 GeV) expecting most of the cross section to be concentrated around the octet electron resonance. (The resolution of $M(jets, e^-)$ is assumed to be $\frac{\Delta M}{M} \approx \frac{1}{2}\frac{\Delta E_{jet}}{E_{jet}} \approx 2.5\%$ and a two sigma deviance is considered.)

In Figures 14, 15 and 16 the normalized invariant mass distribution of the final state positron and electron and the normalized transverse momentum as well as pseudorapidity distributions of the final state jets are presented applying the cuts described above. These normalized distributions do not depend on the value of the compositeness scale, which can be seen from equation (31). To generate the distributions a compositeness scale of 5000 GeV is chosen. Using these distributions the following cuts are chosen for further calculations: $475\,\text{GeV}< M(jets, e^-) < 525\,\text{GeV}$ and $950\,\text{GeV}< M(jets, e^-) < 1050\,\text{GeV}$ for an octet electron mass of 500 GeV and 1000 GeV respectively and $M(e^+, e^-) > 120\,\text{GeV}$, $|\eta(jets)| < 2.5$, $|\eta(e)| < 2.5$, $p_T(jets) > 100\,\text{GeV}$, $p_T(e) > 25\,\text{GeV}$ for both octet electron masses.

In Table 7, the total cut signal and background cross sections at different octet electron masses are presented. To evaluate the statistical significance Equation (35) is used. Table 8 presents the maximum reachable values of the compositeness scale for a 5σ discovery at different color octet electron masses regarding integrated luminosities of $10\,fb^{-1}$, $40\,fb^{-1}$, $100\,fb^{-1}$ and $300\,fb^{-1}$.

The octet electron mass is equal to the maximum compositness scale for a 5σ discovery at a value

of $4.35\,TeV$ for an integrated luminosity of $300\,fb^{-1}$. The cuts selected for this calculation are: $M(e^+, e^-) > 100\,\text{GeV}$, $|\eta(jets)| < 2.5$, $|\eta(e^-)| < 2.5$, $|\eta(e^+)| < 2.5$, $p_T(jets) > 20\,\text{GeV}$, $p_T(e^+) > 10\,\text{GeV}$, $p_T(e^-) > 10\,\text{GeV}$ and $M(jets, e^-) > 3500\,\text{GeV}$.
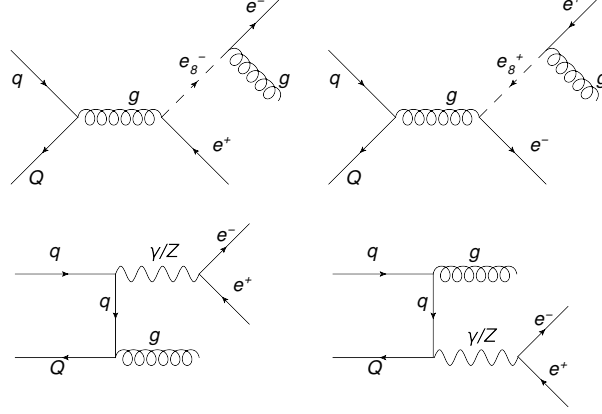
Fig. 12: Feynman diagrams of considered signal and background processes. q represents all quarks except for the top and Q is the corresponding anti quark.
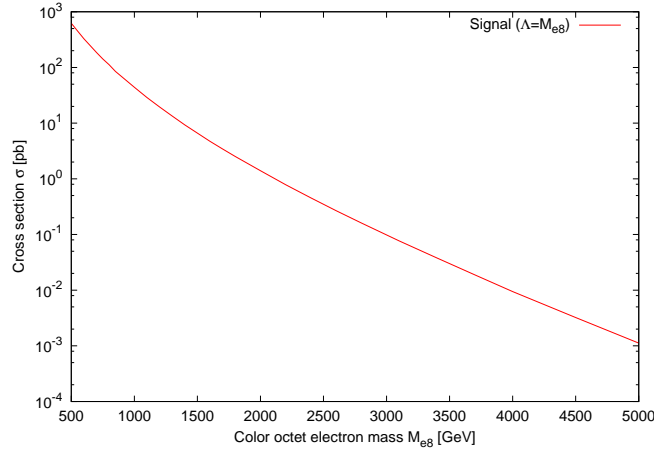
Fig. 13: Cross section for the resonant color octet electron production as a function of the octet electron mass. The following cuts on final state particles are applied: $p_T(e) > 100$ GeV, and $p_T(jets) > 100$ GeV. The center-of-mass energy is assumed to be 14 TeV.

$M_{e8}\ [GeV]$	500	1000
$\sigma_s\ [fb]$	733	139
$\sigma_b\ [fb]$	2.48	0.337

Tab. 7: Signal (σ_s) and background (σ_b) cross sections after cuts for the LHC at different octet electron masses M_{e8}. The compositeness scale is chosen to be 5000 GeV and the center-of-mass energy is assumed to be 14 TeV.

M_{e8}	$10\ fb^{-1}$	$40\ fb^{-1}$	$100\ fb^{-1}$	$300\ fb^{-1}$
500 GeV	60 TeV	100 TeV	130 TeV	180 TeV
1000 GeV	35 TeV	60 TeV	80 TeV	120 TeV

Tab. 8: Maximal reachable value of the compositeness scale Λ for a 5σ discovery at different color octet electron masses M_{e_8} considering different integrated luminosities and a center-of-mass energy of 14 TeV.
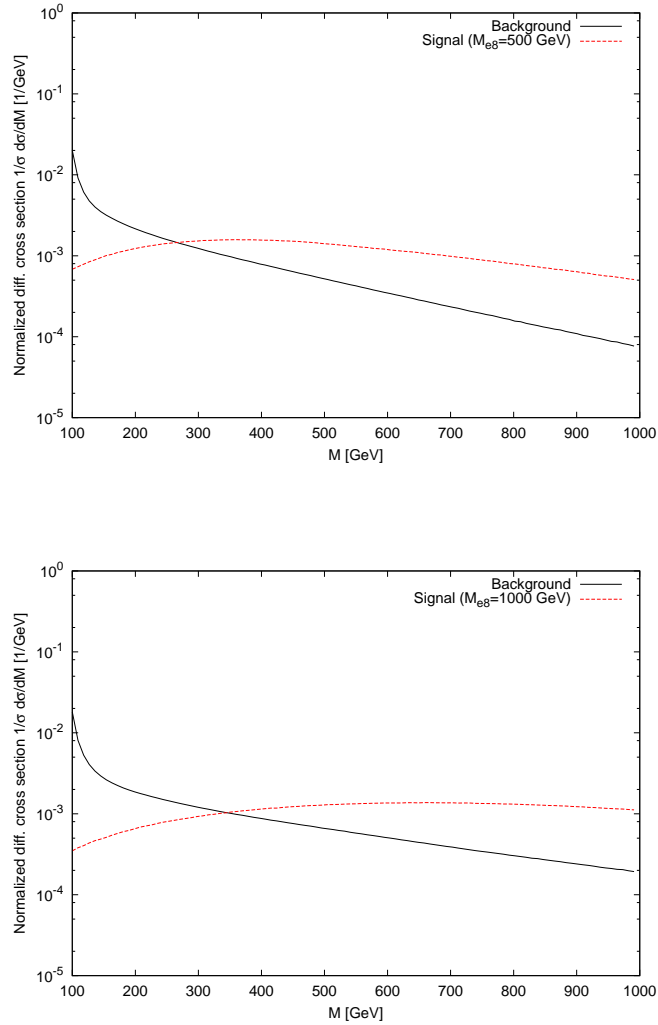
Fig. 14: Normalized signal and background invariant mass distribution of final state electron and positron at different octet electron masses. The compositeness scale is chosen to be 5000 GeV. The center of mass energy is assumed to be 14 TeV.
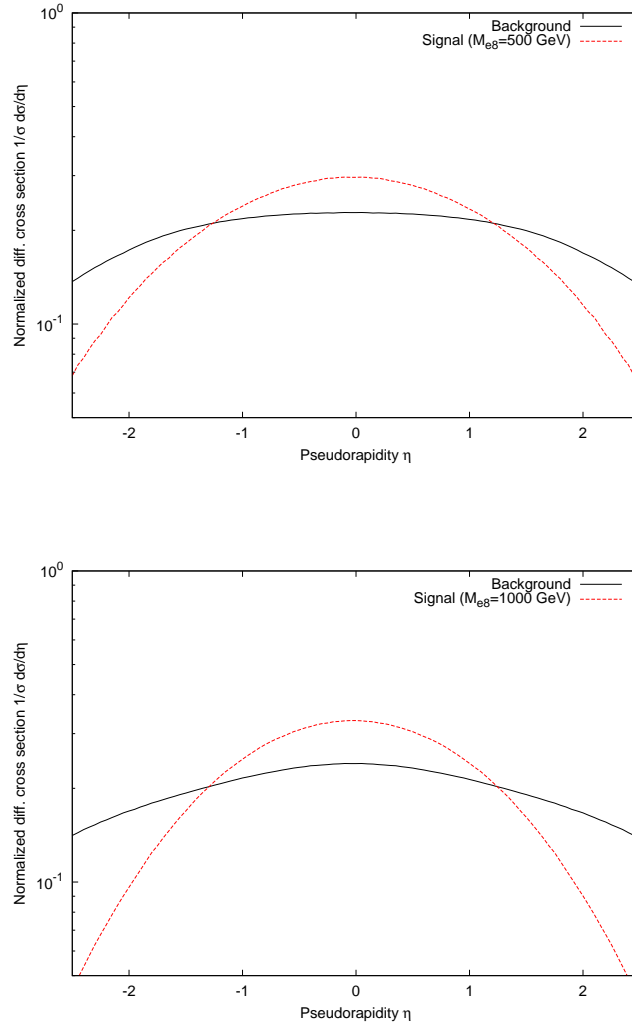
Fig. 15: Normalized signal and background pseudorapidity distribution of final state jets at different octet electron masses. The compositeness scale is chosen to be 5000 GeV. The center of mass energy is assumed to be 14 TeV.
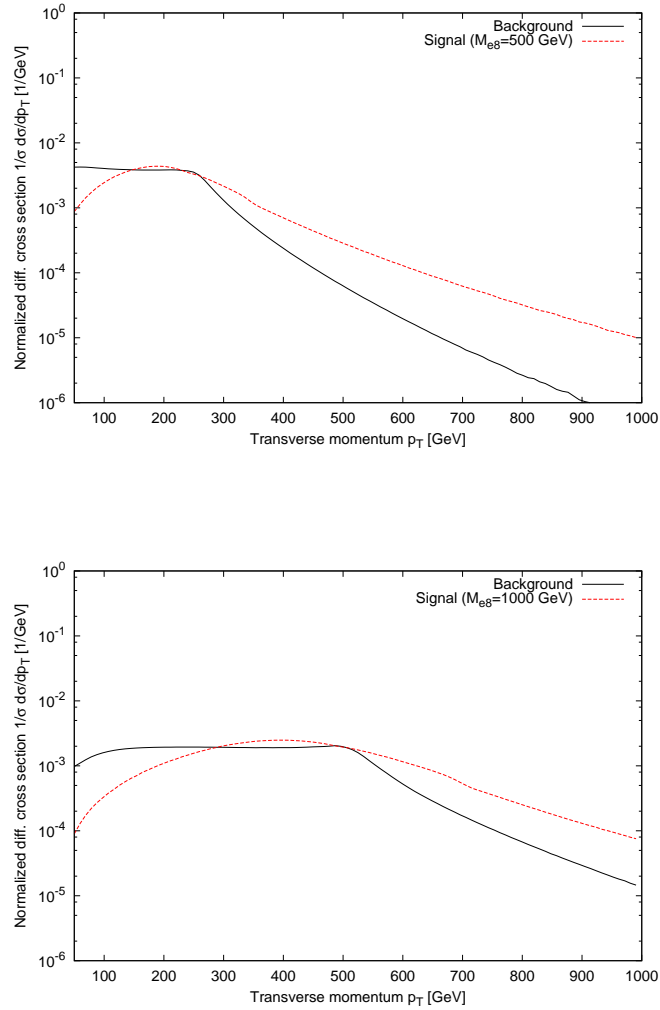
Fig. 16: Normalized signal and background transverse momentum distribution of final state jets at different octet electron masses. The compositeness scale is chosen to be 5000 GeV. The center of mass energy is assumed to be 14 TeV.

5   CONCLUSION AND DISCUSSION

In this study both the indirect ($gg \rightarrow e^+e^-$) and the resonant ($q\bar{q} \rightarrow ge^+e^-$) manifestation of color octet electrons at the LHC's general purpose detectors were investigated.

Considering an integrated luminosity of $300\,fb^{-1}$ and an octet electron mass of 1000 GeV the resonant production at the LHC allows to cover values of the compositeness scale up to approximately 120 TeV whereas the indirect manifestation can merely cover values up to only 8.5 TeV. With growing octet electron mass the indirect manifestation becomes more significant, but at octet electron masses of around 4.35 TeV the resonant production still covers higher compositness scales. The presented studies show that in the search for color octet electrons at the LHC the resonant production is better suited than the indirect manifestation at least up to octet electron masses of approximately 4.35 TeV.

It is of interest to compare the LHC's capacity to discover octet electrons to that of future accelerators [4, 6]. The reachable octet electron mass for a 5σ discovery at the LHC assuming an integrated luminosity of $300\,fb^{-1}$ and a center-of-mass energy of 14 TeV is 4.0 TeV for indirect manifestation and 4.35 TeV for resonant production if the compositeness scale is set equal to the octet electron mass. These values clearly exceed the capacity of CLIC1 ($1.6\,TeV$) [6] and the ILC ($1.6\,TeV$) [6] to discover octet electrons and are also well behind that of CLIC2 ($6.4\,TeV$) [6]. According to M. Sahin et al. [4] the resonant octet electron production at the LHeC/QCDE-2 will cover octet electron masses up to $\mathcal{O}(1700\,\mathrm{GeV})$. Both the indirect and the resonant manifestation of octet electrons at the LHC can cleary exceed this value assuming an integrated luminosity $300\,fb^{-1}$ and a center-of-mass energy of 14 TeV. Considering octet electron masses lower than 750 GeV, the resonant octet electron production at the LHeC seems to enable the coverage of significantly higher compositeness scales compared to the indirect and the resonant octet electron manifestation at the LHC. But since gluon fusion becomes relevant at these masses in case of the resonant production a precise statement is not possible.

Finally, it can be stated that the LHC already has the capacity to deliver essential information approximately the existence octet electrons.

Acknowlegement

6   APPENDIX

Appendix A

CalcHEP [7] is used for the numerical evaluation of the tree-level cross sections. To this end, model files containing all necessary information about the interaction have to be created. LanHEP [13] was used to produce model files for CompHEP which strongly resemble that for CalcHEP. Working with CalcHEP, the files created with LanHEP were used to include octet electrons in the already existing SM model files of CalcHEP. To this purpose some code had to be added to the different model files. In the following these additions are specified:

Additions in the model file that defines particles (prtcls1.mdl):

e8-leptogluon| e8 | E8 |99 | 1 |Me8 |we8 |8 | |e8 |\bar{e8}

Additions in the model file that defines parameters (vars1.mdl):

Me8 |1000 |lg-leptogluon mass

LAMBDA |10000 |compositeness scale

Pi |3.1416 |Pi

In the model file that defines functions of parameters the octet electron decay width given by equation (34) is implemented (func1.mdl):

we8 |alfas*(Me8^3)/(LAMBDA)^2 %width of color octet electron

In the model file that defines vertices the couplings given by Equations (17), (18), (43) and (44) are implemented (lgrng1.mdl):

E |e8 |G | |-GG/(2*LAMBDA) |G(p3)*G(m3)*(1+G5)-G(m3)*G(p3)*(1+G5)

E8 |e |G | |GG/(2*LAMBDA) |G(m3)*G(p3)*(1-G5)-G(p3)*G(m3)*(1-G5)

E |e8 |G |G |i*GG^2/(2*LAMBDA) |G(m4)*G(m3)*(1+G5)-G(m3)*G(m4)*(1+G5)

E8 |e |G |G |i*GG^2/(2*LAMDBA) |G(m4)*G(m3)*(1-G5)-G(m3)*G(m4)*(1-G5)

Appendix B

The two parts of the Lagrangian that give rise to four particle vertices are considered:

$$L_3 = -\frac{ig_s^2}{4\Lambda} \sum_l \bar{\psi}_{l_8} f^{abc} A_\mu^b A_\nu^c [\gamma^\mu, \gamma^\nu](1 - \gamma_5)\psi_l \tag{36}$$

$$L_4 = -\frac{ig_s^2}{4\Lambda} \sum_l \bar{\psi}_l f^{abc} A_\mu^b A_\nu^c [\gamma^\mu, \gamma^\nu](1 + \gamma_5)\psi_{l_8} \tag{37}$$

$L_4(L_3)$ only contributes in the cases that involve incoming $l_8^-(l_8^+)$ or $l^+(l^-)$ or outgoing $l_8^+(l_8^-)$ or $l^-(l^+)$. Figure 17 presents the vertices that correspond to L_3 and L_4. To obtain the couplings an analogous calculation is done:

$$\langle l_8^- | i \int d^4x : L_3(x) : |l^-, g, g\rangle \tag{38}$$

$$= \langle l_8^- | \int d^4x : \frac{g_s^2}{4\Lambda} \sum_l \bar{\psi}_{l_8} f^{abc} A_\mu^b A_\nu^c [\gamma^\mu, \gamma^\nu](1 - \gamma_5)\psi_l : |l^-, g, g\rangle \tag{39}$$

$$= \langle 0 | \frac{g_s^2}{4\Lambda} f^{abc} \int d^4x \, e^{ikx} \bar{u}_{s_1}(k)\delta_{ad}(e^{-iqx}\epsilon_{\mu,\lambda_1}(q_1)\delta_{be}e^{-iux}\epsilon_{\nu,\lambda_2}(q_2)\delta_{cf} +$$

$$e^{-iqx}\epsilon_{\nu,\lambda_1}(q_1)\delta_{ce}e^{-iux}\epsilon_{\mu,\lambda_2}(q_2)\delta_{bf})[\gamma^\mu, \gamma^\nu](1 - \gamma_5)u_{s_2}(p)|0\rangle \tag{41}$$

$$= \bar{u}_{s_1}(k)\frac{g_s^2}{2\Lambda} f^{def}[\gamma_\alpha, \gamma_\beta](1 - \gamma_5)\epsilon_{\alpha,\lambda_1}(q_1)\epsilon_{\beta,\lambda_2}(q_2)u_{s_2}(p) \int d^4x \, e^{i(k-q_1-q_2-p)x} \tag{42}$$

The coupling for L_3 is given by:

$$\frac{g_s^2}{2\Lambda} f^{def} [\gamma_\alpha, \gamma_\beta](1 - \gamma_5) \tag{43}$$

Analogously the coupling for L_4 is found to be:

$$\frac{g_s^2}{2\Lambda} f^{def} [\gamma_\alpha, \gamma_\beta](1 + \gamma_5) \tag{44}$$
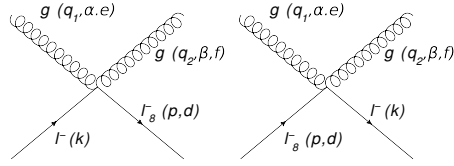
Fig. 17: The left vertex corresponds to L_3 , the right to L_4. p, q_1, q_2 and k denote four-momenta of appropriate particles. All four-momenta may point in the direction of the vertex. d, e and f are color indices. s_1 and s_2 denote spin states. α and β are Lorentz indices of the gluon fields and λ_1 and λ_2 denote their polarization states.

References

[1] I.A. D'Souza and C.S. Kalman. *PREONS Models of Leptons, Quarks and Gauge Bosons as Composite Objects*. World Scientific Publishing Co. Pte Ltd., 1992.

[2] A. Celikel, M. Kantar, and S. Sultansoy. A Search for Sextet Quarks and Leptoguons at the LHC. *Phys. Lett.*, 443B:359–364, 1998.

[3] Michael A. Shupe. A Composite Model of Leptons and Quarks. *Phys. Lett.*, 86B:87–92, 1979.

[4] M. Sahin, S. Sultansoy, and S. Turkoz. Resonant Production of Color Octet Electrons at the LHeC. *arXiv:1001.4505v2 [hep-ph]*, 2010.

[5] H. Fritzsch and G. Mandelbaum. Weak Interaction as Manifestations of the Substructure of Leptons and Quarks. *Phys. Lett.*, 102B:319–322, 1981.

[6] A.N. Akay, H. Karadeniz, M. Sahin, and S. Sultansoy. Indirect Search for Color Octet Electrons at Next Generation Linear Colliders. *arXiv:1012.0189 [hep-ph]*, 2011.

[7] A. Pukov. *arXiv:908288 [hep-ph]*.

[8] M. Peskin and V. Schroeder. *An Introduction to Quantum Field Theory*. Westwind Press, 1995.

[9] S. Martin. A Supersymmetry Primer. *arXiv:9709356v5[hep-ph]*, page 90, 2008.

[10] J. Brau et al. ILC reference design report vol. 3: Accelerator. *ILC-REPORT-2007-001*, 2007.

[11] ATLAS Collaboration. Search for a Heavy Gauge Boson Decaying to a Charged Lepton and a Neutrino in 1 fb^{-1} of pp Collisions at $\sqrt{s} = 7$ TeV Using the ATLAS Detector. *arXiv:1108.1316v1[hep-ph]*, 2011.

[12] J. Pumplin, D.R. Stump, H.L J. Huston, P. Nadolsky Lai, and W.K. Tung. New Generation of Parton Distributions with Uncertainties from Global QCD Analysis. *arXiv:0201195 [hep-ph]*, 2002.

[13] A. Semenov. LanHEP - a package for automatic generation of Feynman rules from the Lagrangian. updated version 3.1. *arXiv:1005.1909v1 [hep-ph]*, 2010.